This is the accepted manuscript made available via CHORUS. The article has been published as:

Propagation uniqueness in three-dimensional coherent diffractive imaging

Xiaojing Huang, Ross Harder, Gang Xiong, Xiaowen Shi, and Ian Robinson

Phys. Rev. B **83**, 224109 — Published 24 June 2011

DOI: 10.1103/PhysRevB.83.224109

Propagation Uniqueness in 3D Coherent Diffractive Imaging

Xiaojing Huang,[1,2] Ross Harder,[2] Gang Xiong,[1] Xiaowen Shi,[1] and Ian Robinson[1,3,*]

[1] *London Centre for Nanotechnology, University College London, London WC1H 0AH, UK*
[2] *Advanced Photon Source, Argonne National Laboratory, Argonne IL 60439, USA*
[3] *Research Complex at Harwell, Didcot, Oxfordshire OX11 0DE, UK*

Propagation non-uniqueness in three-dimensional (3D) coherent diffractive imaging (CDI) arises from the fact that an ensemble of solutions, related by propagation, gives an identical far-field diffraction intensity. Tight support constraint and tight allowed phase range behave similarly in constraining the solution of phase retrieval process, thus removing this non-uniqueness in simple cases, but not for strong phase objects. For CDI in Bragg geometry, we introduce a two-step phasing procedure for reconstructing heavily-strained samples, which balances the need to define both support and phase constraints.

PACS numbers: 87.59.-e, 61.05.cp, 42.30.Rx, 61.46.-w

Coherent Diffractive Imaging (CDI) has made major advances in the past few years [1–4] and has become one of the most exciting applications of the new Free-Electron Laser X-ray sources [5, 6]. The method relies on the ability to determine retrospectively the unknown phases of a measured diffraction pattern [7] and thereby invert those data by Fourier transformation. This is a mathematically overdetermined problem so long as the diffraction pattern is oversampled with respect to its highest spatial frequency [8]. This situation occurs naturally for small, isolated samples where the method is found to work well, with many published examples [9–14]. Most of these examples have 2D or 3D diffraction patterns. Bates showed in 1982 [15] that the 1D Fourier amplitude inversion problem was prone to non-uniqueness corresponding to factorisation of the amplitude function. Non-uniqueness of the 2D and 3D cases was declared to be pathologically rare [16].

The CDI method with Bragg geometry [17] provides a powerful non-destructive tool for 3D imaging strain fields of crystals on the nanometer length scale. In this method, the measured x-ray diffraction pattern surrounding a Bragg peak of a strained crystal can be decomposed into symmetric and antisymmetric parts. To a good approximation, the symmetric part can be considered to come from the shape of the crystal, while the antisymmetric part arises from a real-space phase identified with a projection of the lattice distortions onto the Bragg peak direction about which the diffraction pattern is measured [17].

In this letter, we demonstrate that CDI of strong phase objects is naturally prone to non-uniqueness, even in the 2D and 3D cases. We have found empirically, both here and quite generally in other examples, that diffraction patterns of objects with real-space phase ranges exceeding π are difficult to invert and tend to display density "gaps" in the resulting images where the phase apparently goes out of range. We illustrate this with examples of diffraction patterns of Silicon-on-Insulator (SOI) wire structures in which phase wrapping occurs at sample defects. We have discovered a new phasing procedure which solves the problem by substituting the real-space phase constraint with a tight real-space support constraint. We can see how it works by first understanding the origin of the non-uniqueness for strong-phase objects.

The general 3D CDI problem considers the sample to be $t(\mathbf{r}) = \rho(\mathbf{r})e^{i\phi(\mathbf{r})}$, a real-space density/phase function of position $\mathbf{r}$ whose spatial extent is confined to a well-defined support volume $\mathbf{r} \in \mathbf{S}$. The classical CDI experiment measures the magnitude of the amplitude of the Fourier transform of $t(\mathbf{r})$ as the far-field Fraunhofer diffraction pattern, $A(\mathbf{q})$. Inversion of these data is usually found to be possible if the diffraction pattern is sufficiently oversampled [8]. The usual inversion methods involve algorithms that cycle between real and reciprocal space, asserting an estimate of $\mathbf{S}$ and the measured $|A(q)|$ respectively [18]. These are found to work reliably, so long as the phase of the sample is not too strong (typically $|\phi(\mathbf{r})| \leq \frac{\pi}{2}$ in practice), and appear to give unique 3D solutions in simple cases.

We refer to the particular kind of non-uniqueness considered here as propagation non-uniqueness. We are ignoring other known sources of non-uniqueness, including the trivial symmetries of the Fourier transform and the factorization problem referred to above [15]. Propagation non-uniqueness is most easily understood in the 2D case, involving free-space propagation between planes. Here we can think of $t(\mathbf{r})$ as the complex amplitude of the electromagnetic wave exiting from the sample, spanned by a 2D transverse position vector $\mathbf{r}$ and illuminated by a plane wave of wave vector $\mathbf{k}$ along the optical axis. $A(\mathbf{q})$ is the resulting Fourier transform, whose magnitude is detected in the far field. At any distance d beyond the sample, the wavefront will have evolved by classical wave propagation to

$$t'(\mathbf{r}') = \int t(\mathbf{r}) e^{-ik(\mathbf{r}-\mathbf{r}')^2/2d} d\mathbf{r}, \qquad (1)$$

where $\mathbf{r}'$ is the 2D position within the new plane. When this same wave continues to propagate all the way to

the detector, it becomes $A(\mathbf{q})$ again in the far-field (except for a phase offset). It is clear from this argument that both $t(\mathbf{r})$ and $t'(\mathbf{r}')$ have the same Fourier transform modulus $|A(\mathbf{q})|$, hence the inversion of $|A(\mathbf{q})|$ is non-unique.

The 3D generalization of Eq. 1 is mathematically simple, but no longer easy to visualize as mere selection of the focal plane. A general set of non-unique objects can be obtained by propagating different distances d in the x, y or z directions (or in between). These objects are all indistinguishable in CDI.

To see why CDI works at all, we need to examine the properties of the set of propagated non-unique structures generated by Eq. 1, which all have the same Fourier transform. For example, if $t(\mathbf{r})$ is a real box function, $t'(\mathbf{r}')$ is the familiar Fresnel integral, resembling an out-of-focus image of the box but with strongly phased fringes at the edges. If $t(r)$ is a real Gaussian, $t'(\mathbf{r}')$ is also a wider Gaussian but with quadratically curved phase with $\phi(\mathbf{r}') = k(\mathbf{r}')^2/2d$. The general behavior of real objects under Eq. 1 is: 1) they become broader (out of focus) and 2) the phase becomes stronger. It is clear from this why real objects are easy to solve when their phase can be constrained to a narrow or zero range. A tight support is also effective because it excludes the spread-out, propagated versions of the object [19]. For objects with relatively small phase variation range, adding a phase constraint to the standard HIO algorithm significantly increases the reconstruction efficiency, but only with a phase range up to $\Phi = [-\pi/2, \pi/2]$ [20]. This phase-constrained hybrid input-output (PCHIO) algorithm can be expressed as:

$$g^{(n+1)}(\mathbf{r}) = \begin{cases} \mathbf{p_m} g^{(n)}(\mathbf{r}), & \mathbf{r} \in \mathbf{S} \text{ and } \phi(\mathbf{r}) \in \Phi, \\ \mathbf{p_m} g^{(n)}(\mathbf{r}) - \beta g^{(n)}(\mathbf{r}), & \text{otherwise,} \end{cases} \quad (2)$$

where $g^{(n)}$ is the current iteration output, $\mathbf{p_m}$ is the Fourier modulus constraint projection, β is the feedback constant, $\mathbf{S}$ and Φ denote the support region and the phase constraint range. A typical $[-\pi/2, \pi/2]$ phase range gives robust reconstructions with loose box supports for weakly strained samples [2, 20, 21].

A numerical experiment was carried out to understand why the phase constraint is efficient to give reliable reconstructions even with loose support. Similar to the one used by Spence *et. al.* [19], the simulated system consists of two planes separated along propagation direction by 100 μm (Fig. 1(a)). Letter A and B are on the upstream plane, and have quadratic phase structure within the range $[0, \pi/6]$. Letter C is located on the downstream plane with $[0, \pi/3]$ quadratic phase. Far-field diffraction pattern was calculated from the exit wave at the downstream plane (Fig. 1(b)). Reconstructed images show that the upstream plane comes into focus when either a tight support (Fig. 1(c)) or a tight allowed phase range (Fig. 1(e)) is applied, while Letter C is out of focus. The downstream plane is selected when the support or phase range match that plane (Fig. 1(d)(f)). This simulation shows that a unique solution can be determined by either a tight support or a tight allowed phase range and that the propagation non-uniqueness can be removed either way.

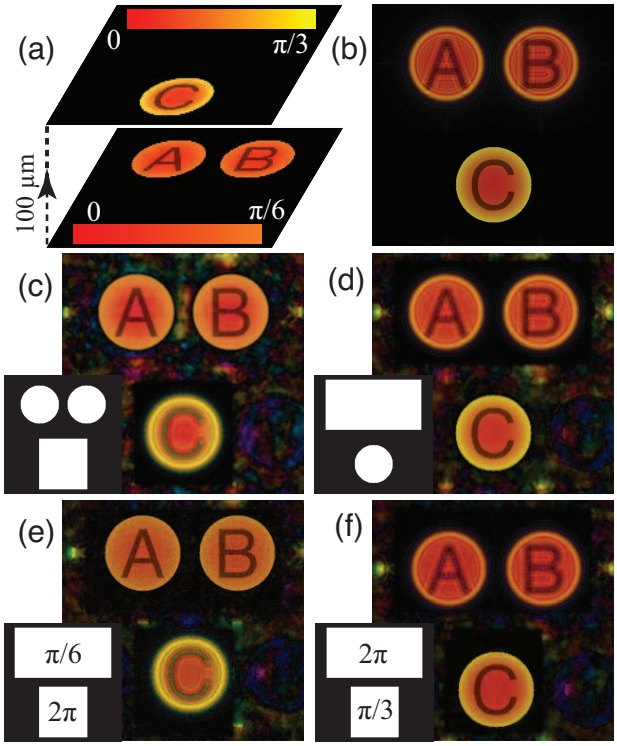

FIG. 1: Simulated reconstruction of a compound complex object located in two distinct planes with 9 keV x-rays ($\lambda = 0.138$ nm). (a) Letters A and B are in the same plane and contain quadratic phase structure within the range $[0, \pi/6]$. Letter C is located 100 μm downstream with $[0, \pi/3]$ quadratic phase. (b) The simulated exit wave magnitude at Letter C plane. (c)(d) Tight supports with no phase constraint select which plane comes into focus in the CDI reconstructed image, as found by Spence *et. al.*[19]. (e)(f) A constraint on the allowed phase range also defines the focal plane with loose supports. The support and allowed phase range for each reconstruction condition are shown schematically as insets.

For strong phase objects, however, we no longer have the luxury of selecting a focal plane to break the non-uniqueness. We can use a tight support constraint to find the solution with the smallest width. But it might not be correct, since propagation by Eq. 1, or the more general version in 3D, can sometimes make the object smaller, as is the case for a Fresnel Zone Plate, for example. Without further real-space information, the solution is just limited to a range of possibilities, interconnected by generalized 3D propagation. Fortunately, we often do have real-space information about the sample which can be applied to pick the "correct" solution from the ensemble. In general this might require the incorporation of some real-space model to guide the solution; for example, the phase could

be limited to a range $\leq \pi$ at each position within the sample, but centered around a model-determined value. In this paper, we illustrate a new method in which a tight support is generated first, then applied with relaxed phase range.

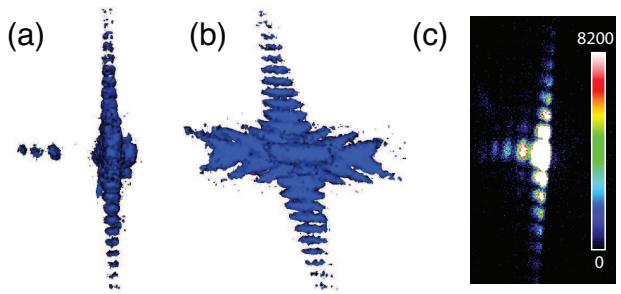

FIG. 2: (a)(b) 3% iso-surface of the diffraction pattern from a SOI wire section viewing along x and z directions. (c) A typical central frame of diffraction pattern from the same SOI wire.

We chose lithographed SOI patterns for our test samples because SOI has the potential for producing high performance semiconductor devices [22], and it offers the opportunity for strain engineering to enhance electron mobility [23]. We used SOI wafers with (001) silicon top layer, 700 nm thick, wafer-bonded to a (111) silicon substrate. The designed pattern was "wires" of 15 μm length and widths varying from 500 nm to 1500 nm, sculptured using electron-beam lithography followed by reactive ion etching. The CDI experiment was performed at Advanced Photon Source beamline 34-ID-C, Argonne National Laboratory. A 9 keV coherent x-ray beam was selected by a silicon (111) double crystal monochromator and slits. The coherent x-ray beam was focused to about 2 μm using Kirkpatrick-Baez mirrors. 3D diffraction patterns surrounding (111) Bragg peaks were measured by rotating the sample and thus the entire diffraction pattern across a charge-coupled-device (CCD) detector slice by slice. The sample was rotated by 0.6 degree with 100 angular steps. The CCD detector with 22.5 μm pixel size was placed 1.5 m away from the specimen. The measured diffraction patterns were subsequently inverted using the PCHIO iterative phase retrieval algorithm in Eq. 2 to obtain real space images [18, 20]. The cropped data array that was used for reconstruction gives a voxel resolution of $38 \times 27 \times 60$ nm.

By searching around the sample, a section of SOI wire containing a strong phase defect was identified by its asymmetric diffraction pattern as shown in Fig. 2 (a)(b). Fig. 2 (c) shows a typical central frame of diffraction data from this SOI wire. Since the imaged wires are longer than the x-ray illumination size, the length of phased SOI sections is determined by the focal size of the x-ray beam which is about 2 μm. We found that the image magnitude is unable to be determined at the positions where the phase variations are beyond the defined range $[-\pi/2, \pi/2]$ in PCHIO, leading to missing density especially at the places where the real-space phase varies strongly (Fig. 3 (a)–(d)), which is physically unreasonable. By locally removing this $[-\pi/2, \pi/2]$ phase constraint or increasing the allowed phase range to $[-\pi, \pi]$, the missing sections were found to fill in, but the overall boundaries of the obtained structures became coarse, and their cross-section shape differed from the expected wedged profile caused by an undercutting effect of the etching process. This is apparently because the loose support and lack of phase constraint are insufficient to resolve the propagation uniqueness, as illustrated in our tests. Applying the "shrink-wrap" method [24] directly did not produce decent reconstructions either.

We noticed that although the PCHIO algorithm could not retrieve the entire structure, it gave well defined boundaries for those sections with relatively small phase variations (Fig. 3 (b)). A refined support was generated from this reconstruction using the same method as in "shrink-wrap" [24] by blurring the image with a Gaussian function and setting a magnitude threshold. The blurring width and threshold were adjusted to obtain a tight-fitting support with the desired wedged shape and continuous over the full length of the wire. To increase the confidence of the refined support, preliminary reconstructions were run 10 times with individual random starts. These 10 images obtained were classified into two groups: one with the regular orientation and the other with the enantiomorphous orientation. The images in the second group were then spatially flipped in 3D and complex-conjugated. The orientation-corrected images were then shifted and aligned with each other [27]. We averaged all 10 images together and applied shrink wrap to produce a refined tight support. Individual random starts give consistent phased images using this support.

We then ran regular HIO without phase constraint and with this refined support. The resulting images had smooth boundaries, and continuous density at the locations with severe phase changes as shown in Fig. 3 (e-h). This physically reasonable finding of solid wire-shaped images with a localized phase jump, attributed to a planar lattice defect such as a slip plane, confirms that we have successfully resolved the propagation uniqueness in this example. The result compares favorably with recently developed algorithms enforcing a uniformity constraint [25] or utilizing compressive sensing theory [26].

To investigate the influence of incident x-ray beam on the phase structure, different sections of the same SOI wire were measured in sequence under the same experimental condition. We found that this 2π phase wrapping only happens at some locations of the wire, while other sections give smooth and continuous magnitude structure with moderate phase variation range less than $[-\pi/2, \pi/2]$. This implies that the phase structures mainly come from the SOI wires. Completely factorizing the x-ray beam profile out of the reconstructed image

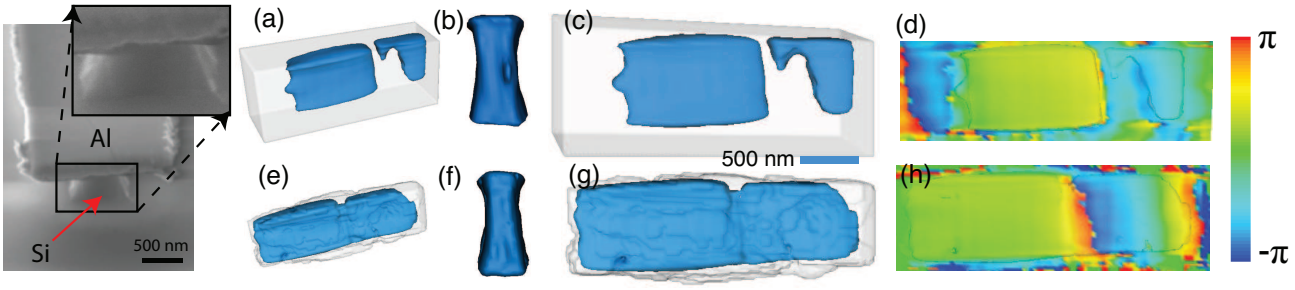

FIG. 3: The SEM image of a 1200 nm SOI wire shows a wedged cross-section due to undercutting in the etching process. 9% iso-surface renderings of reconstructed magnitudes (a)-(c) and phase (d) of a 900 nm SOI wire section with a box support and the PC-HIO algorithm with $[-\pi/2, \pi/2]$ phase range averaged from aligned 10 reconstructions. 9% iso-surface renderings of reconstructed magnitudes (e)-(g) and phase (h), reconstructed with our method from the same data set with a support refined from previous reconstruction and no phase constraint.

requires ptychographic approaches [4].

In our investigations of CDI phase retrieval of complex objects, we have found it necessary to employ a significant phase constraint or else a closely matching support to avoid propagation non-uniqueness. Our simulation in Fig. 1 confirms that such a phase constraint works as efficiently as a tight support constraint. This result explains both why propagation uniqueness problems have not emerged before for weak-phase objects and why strong phase objects have proved so difficult to invert. We have demonstrated a new two-step phasing procedure which first reconstructs the shape of an object using a finite phase constraint and loose support, then refines a tight support from the pre-reconstructed image with which the final reconstruction using standard HIO algorithm can be performed. This method balances the difficulties of determining accurate support and phase constraints. It should greatly extend the capability of Bragg CDI for the previously difficult case of highly strained crystals.

This work was supported by FP7 "advanced" grant from the European Research Council. The experimental work was carried out at Advanced Photon Source Beamline 34-ID-C, built with funds from the US National Science Foundation under Grant DMR-9724294 and operated by the US Department of Energy, Office of Science, Office of Basic Energy Sciences, under Contract DE-AC02-06CH11357.

* Electronic address: i.robinson@ucl.ac.uk

[1] J. Miao *et al.*, Nature **400**, 342 (1999).
[2] M. Pfeifer *et al.*, Nature **442**, 63 (2006).
[3] G. Williams *et al.*, Phys. Rev. Lett. **97**, 025506 (2006).
[4] P. Thibault *et al.*, Science **321**, 379 (2008).
[5] H. Chapman *et al.*, et al., Nature Phys. **2**, 839 (2006).
[6] A. Barty *et al.*, et al., Nature Photon. **2**, 415 (2008).
[7] D. Sayre, in *Imaging Processes and Coherence in Physics*, edited by M. Schlenker *et al.* (Springer-Verlag, Berlin, 1980), pp. 229–235.
[8] J. Miao *et al.*, J. Opt. Soc. Am. A **15**, 1662 (1998).
[9] J. Miao *et al.*, Proc. Natl. Acad. Sci. U.S.A. **100**, 110 (2003).
[10] G. Williams *et al.*, Phys. Rev. Lett. **90**, 175501 (2003).
[11] D. Shapiro *et al.*, Proc. Natl. Acad. Sci. U.S.A. **102**, 15343 (2005).
[12] H. Chapman *et al.*, et al., J. Opt. Soc. Am. A **23**, 1179 (2006).
[13] Y. Nishino *et al.*, Phys. Rev. Lett. **102**, 018101 (2009).
[14] H. Jiang *et al.*, Proc. Natl. Acad. Sci. U.S.A. **107**, 11234 (2010).
[15] R. H. T. Bates, Optik **61**, 247 (1982).
[16] M. H. Hayes, IEEE Trans. Acoust. Speech Signal Process. **30**, 140 (1982).
[17] I. Robinson and R. Harder, Nature Mater. **8**, 291 (2009).
[18] J. Fienup, Appl, Opt. **21**, 2758 (1982).
[19] J. Spence *et al.*, Phil. Trans. R. Soc. A **360**, 875 (2002).
[20] R. Harder *et al.*, New J. Phys. **12**, 035019 (2010).
[21] M. C. Newton *et al.*, Nature Mater. **9**, 120 (2010).
[22] G. K. Celler and S. Cristoloveanu, Appl. Phys. Rev. **93**, 4955 (2003).
[23] J. Welser *et al.*, IEEE Electron Dev. Lett. **15**, 100 (1994).
[24] S. Marchesini *et al.*, Phys. Rev. B **68**, 140101 (2003).
[25] A. A. Minkevich, *et al.*, Phys. Rev. B **76**, 104106 (2007).
[26] M. C. Newton *et al.*, Phys. Rev. B **82**, 165436 (2010).
[27] M. Guizar-Sicairos *et al.*, Opt. Lett. **33**, 156 (2008).